Article

Morphology, Structure and Mechanical Properties of Copper Coatings Electrodeposited by Pulsating Current (PC) Regime on Si(111)

Ivana O. Mladenović [1], Jelena S. Lamovec [1], Dana G. Vasiljević Radović [1], Rastko Vasilić [2], Vesna J. Radojević [3] and Nebojša D. Nikolić [4,*]

[1] ICTM—Department of Microelectronic Technologies, University of Belgrade, Njegoševa 12, 11 000 Belgrade, Serbia; ivana@nanosys.ihtm.bg.ac.rs (I.O.M.) jejal@nanosys.ihtm.bg.ac.rs (J.S.L.); dana@nanosys.ihtm.bg.ac.rs (D.G.V.R.)
[2] Faculty of Physics, University of Belgrade, Studentski Trg 12-16, 11 000 Belgrade, Serbia; rastko.vasilic@ff.bg.ac.rs
[3] Faculty of Technology and Metallurgy, University of Belgrade, Karnegijeva 4, 11 000 Belgrade, Serbia; vesnar@tmf.bg.ac.rs
[4] ICTM—Department of Electrochemistry, University of Belgrade, Njegoševa 12, 11 000 Belgrade, Serbia
* Correspondence: nnikolic@ihtm.bg.ac.rs; Tel.: +381-11-337-0390

Received: 10 March 2020; Accepted: 3 April 2020; Published: 7 April 2020

Abstract: Copper electrodeposition on (111)-oriented Si substrate was performed by the pulsating current (PC) regime at various average current densities in the range of 15–70 mA·cm^{-2}, obtained by varying either the frequency (30, 50, 80 and 100 Hz for the current density amplitude of 100 mA·cm^{-2}) or the current density amplitude (120 and 140 mA·cm^{-2} at 100 Hz). The produced Cu coatings were examined by SEM, AFM and XRD techniques. The morphology of the coatings changed from those with large grains to fine-grained and globular, while the crystal structure changed from the strong (220) to the strong (111) preferred orientation by increasing the average current density. The mechanical characteristics of coatings were examined using Vickers micro-indentation tests, applying the Chicot–Lesage (C–L) composite hardness model for the analysis of microhardness. The maximum microhardness was obtained for the Cu coating produced at an average current density of 50 mA·cm^{-2}, with a current density amplitude of 100 mA·cm^{-2} and a frequency of 100 Hz. This copper coating was fine-grained and showed the smallest roughness in relation to the other coatings, and it was obtained in the mixed activation–diffusion control between the end of the effect of the activation control and the beginning of the dominant effect of diffusion control.

Keywords: copper; electrodeposition; the pulsating current (PC) regime; morphology; microstructure; composite hardness.

---

1. Introduction

Nanocrystalline materials, and in particular metals, whose grain sizes do not exceed 100 nm, have become attractive for use in various industries due to their specific physicochemical and mechanical properties. Several techniques are known for the synthesis of nanocrystalline materials in the form of thin films or coatings on various substrates: chemical vapor deposition (CVD), physical vapor deposition (PVD), electrochemical deposition (ED), electroless deposition (EL), etc. [1]. Physical methods for deposition of thin films, such as sputtering or evaporation, are limited in terms of film thickness, intended for thin films of less than 1–2 µm [2]. Unlike physical methods, there are no restrictions on the thickness of the film during the application of electrodeposition methods.

For application in Micro-Electromechanical Systems (MEMS) technologies, thin films and coatings must have good adhesion to the substrate, good corrosion resistance and good wear resistance, while maintaining satisfactory mechanical properties [3–7]. In MEMS technologies, the processes of the formation of uniform and compact Cu films and coatings are applied in the production of inductive copper micro-coils for magnetic particles detection [8], in combination with micro-machining techniques to obtain micro-gear [9], for wiring on printed circuit boards (PCBs) and bottom-up filling or superfilling techniques for fabrication of Through Silicon Via (TSV) structures [10]. In addition, copper coatings are used as sacrificial layers for the production of different laminar composite structures [11]. Aside from MEMS technologies, various processes of Cu deposition also found a wide application in microelectronic packaging and interconnects [12,13].

For all the above-mentioned applications, good film quality at the micro- or nano-level is required, and electrodeposition processes are very suitable to reach it. In relation to the application of constant regimes of electrolysis, the improvement of the quality of Cu coatings, i.e., their morphological and structural characteristics, can be achieved by the application of electrodeposition at a periodically changing rate [14–16], and the addition of specific substances known as additives to the electroplating baths [17–19], or simply by the regulation of parameters of electrolysis including mixing of the electrolyte, finding of the optimal temperature for electrodeposition or balanced salt/acid contents when acidic baths are used [20,21].

One of the most important mechanical characteristics of metal films and coatings is microhardness, which is closely dependent on processing parameters used for their production [22,23]. Examining the mechanical response of a composite system constructed from substrate and film or coating on indentation and estimating the absolute film hardness independently from the substrate hardness include knowledge of parameters and phenomena such as type of the composite system [24], applied load, duration of the applied load at indentation (dwell time) and indentation depth [25,26], thickness of the coatings [27], elastic properties of the coatings [28], indentation size effect (ISE) [29–32], interfacial adhesion [33,34], etc. A large number of mathematical composite models have been developed so far to determine the "true" or absolute hardness of the film [27,32–36].

In this study, morphological, structural and mechanical characteristics of Cu coatings electrodeposited on Si(111) substrate by the pulsating current (PC) regime were examined. This was done with the aim to define working conditions enabling the formation of uniform and compact coatings of high microhardness. For that purpose, parameters of the PC regime, such as the current density amplitude and frequency (pause duration), were analyzed. The thickness of the coatings was also examined. The composite hardness model of Chicot–Lesage (C–L) was chosen and applied to experimental data in order to analyze the composite systems made [27,35,36]. The basis of the theory of the composite hardness model according to Chicot–Lesage (C–L) is given in Appendix A.

2. Materials and Methods

Electrodeposition of copper was performed from 240 $g \cdot L^{-1}$ $CuSO_4 \cdot 5H_2O$ in 60 $g \cdot L^{-1}$ H_2SO_4 at room temperature by the regime of pulsating current (PC). Analytical grade chemicals and doubly distilled water were used for the preparation of the electrolyte. The parameters of the PC regime used in the electrodeposition processes are given in Table 1.

The working conditions were selected to enable the formation of compact deposits with uniform current density distributions without stirring of the electrolyte. The thickness of all Cu coatings mentioned in Table 1 was 40 μm. The coatings with different thicknesses of 10, 20 and 60 μm were additionally made under the conditions given for Sample 1.

In all experiments, Si(111) wafers (2", p-type, thickness 300 ± 15 μm), cut as pieces with a total surface area of 2 cm^2, were used as the substrate (cathode) for the electrodeposition process. The preparation of Si(111) wafers as a cathode was performed according to the standard MEMS procedure [37], by the formation of thin layers of Cr (30 nm) and Au (100 nm) on Si as adhesion and nucleation layers by the sputtering procedure, using the Perkin Elmer 2400 sputtered system

(PerkinElmer Corporation, Massachusetts, MA, USA). The surface area for Cu electrodeposition was 1 cm^2. A high purity copper plate was used as the anode. The Si(111) plate prepared for the electrodeposition was situated in the middle of the cell between two parallel Cu plates.

For this electrolyte, the polarization curve was recorded by the potentiostatic method using working, reference and counter electrodes of pure copper [38].

Table 1. The parameters of the pulsating current (PC) regime used in the electrodeposition processes. j_A—the current density amplitude, t_c—deposition time (on period), t_p—pause time (off period), p—the pause-to-pulse ratio, j_{av}—the average current density and ν—frequency.

Number of Samples	j_A/mA·cm^{-2}	t_c/ms	t_p/ms	p	j_{av}/mA·cm^{-2}	ν/Hz
1	100	5	5	1	50	100
2	100	5	7.5	1.5	40	80
3	100	5	15	3	25	50
4	100	5	28.3	5.66	15	30
5	120	5	5	1	60	100
6	140	5	5	1	70	100

Characterization of the Produced Cu Coatings

Characterization of the produced Cu coatings was performed by the following techniques:

(a) The morphology of the Cu coatings was examined by scanning electron microscope (SEM)—model JEOL JSM-6610LV (JEOL Ltd., Tokyo, Japan).

(b) The X-ray diffraction (XRD) analysis of the Cu coatings was performed applying RIGAKU Ultima IV diffractometer (Rigaku Co. Ltd., Tokyo, Japan) in Bragg–Brentano Geometry with CuKα radiation in a 2θ range from 30° to 95°.

The preferred orientation of Cu coatings was estimated by determining the "Texture Coefficient", *TC*(*hkl*) and the "Relative Texture Coefficient", *RTC*(*hkl*) [39–41]. The procedure for the determination of these coefficients is described in Appendix B.

(c) The surface topography of the Cu coatings of 70 × 70 μm^2 scan area was examined using an atomic force microscope (Auto Probe CP Research; TM Microscopes, Veeco Instruments, Santa Barbara, CA, USA) in the contact mode. The values of the arithmetic average of the absolute (R_a) roughness parameters were measured from the mean image data plane, using software SPLab (SPMLab NT Ver. 6.0.2., Veeco Instruments, Santa Barbara, CA, USA).

(d) The mechanical characteristics of the Cu coatings were characterized using Vickers microhardness tester Leitz Kleinert Prufer DURIMET I (Leitz, Oberkochen, Germany) with loads ranging from 2.942 N down to 0.049 N. The dwell time was 25 s. Measurements were performed at room temperature. For each load, three indentations were made and the diagonals of the indents were measured by an optical microscope (Olympus CX41; Olympus Corporation, Tokyo, Japan) connected to the computer. With the mean value of the diagonal of the indent, the value of the composite hardness could be calculated for each load. The Chicot–Lesage (C–L) composite hardness model was used to analyze the obtained experimental data.

3. Results

3.1. Basic Facts Necessary for Understanding of the Presented Results

The square wave pulsating current (PC) regime is defined by Equation (1) [42,43]:

$$j_{av} = \frac{j_A \cdot t_c}{t_c + t_p} \tag{1}$$

or

$$j_{av} = \frac{j_A}{1 + p} \tag{2}$$

If

$$p = \frac{t_p}{t_c} \tag{3}$$

where j_{av} is the average current density, j_A is the current density amplitude, t_c is deposition pulse (on period), t_p is pause duration in which the system relaxes (off period) and p is the pause-to-pulse ratio.

The PC regime is efficient in a frequency range between 10 and 100 Hz, in which the surface concentration of depositing ions is only determined by the average current density [42,43]. In this frequency range, the surface concentration of depositing ions is constant and equal to that of the constant regime at the current density corresponding to the average current density in the PC regime. From the point of view of the application of this regime, it means that the electrodeposition process by the PC regime in the millisecond range occurs at the average current density.

The polarization curve for copper electrodeposition from 240 g·L^{-1} $CuSO_4·5H_2O$ in 60 g·L^{-1} H_2SO_4 is shown in Figure 1. The ends of the activation control and the mixed activation–diffusion control (i.e., the beginning of the plateau of the limiting diffusion current density) are denoted by vertical lines in this Figure. The end of the activation control corresponds to an overpotential of 100 mV, while the end of the mixed activation–diffusion control corresponds to an overpotential of 500 mV.

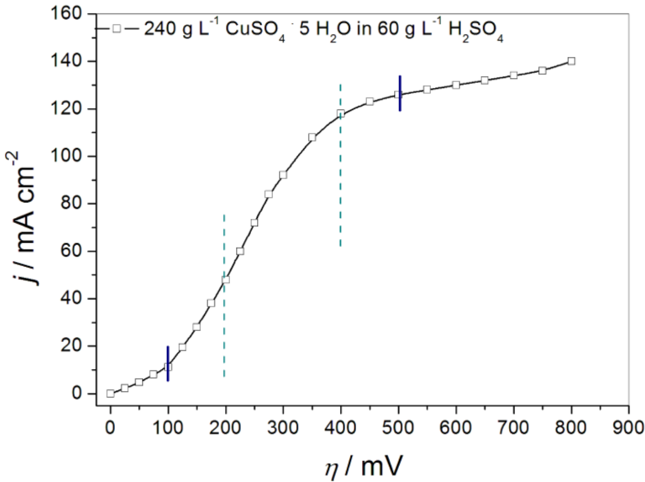

Figure 1. Polarization curve for Cu electrodeposition from 240 g·L^{-1} $CuSO_4·5H_2O$ in 60 g·L^{-1} H_2SO_4.

3.2. Morphology of the Cu Coatings Obtained by Application of the PC Regime

Figure 2 shows morphologies of the Cu coatings obtained at frequencies of 30 Hz (Figure 2a,b), 50 Hz (Figure 2c,d), 80 Hz (Figure 2e,f) and 100 Hz (Figure 2g,h). These frequencies were obtained by a regulation of pause duration keeping a constant amplitude of the current density and the deposition pulse (Table 1).

The Cu coating obtained at a frequency of 30 Hz was very coarse, with large and relatively well-defined crystal grains (Figure 2a,b). The Cu crystals up to about 10 μm in size were formed by this PC regime. The coarseness of the coatings decreased by increasing the frequency, as seen from Figure 2c–h. The smaller number of larger Cu grains (up to 10 μm in size) was obtained with an applied frequency of 50 Hz relative to 30 Hz (Figure 2c,d). The majority of the grains were about 5 μm. The coatings obtained with frequencies of 80 and 100 Hz (Figure 2e–h) were smoother than those obtained with frequencies of 30 and 50 Hz. A further decrease in crystal size and an increase in the uniformity of the coatings was observed by increasing the frequency. In coatings obtained at 80 and 100 Hz, the average crystal size was below 5 μm.

Figure 3 shows the morphologies of Cu coatings obtained with amplitudes of the current density of 120 mA·cm^{-2} (Figure 3a,b), and 140 mA·cm^{-2} (Figure 3c,d). In this series of experiments, the frequency of 100 Hz (t_c = 5 ms and t_p = 5 ms) is kept constant (Table 1). Please note that the coating shown in Figure 2g,h is obtained with an amplitude of 100 mA·cm^{-2} at the same frequency.

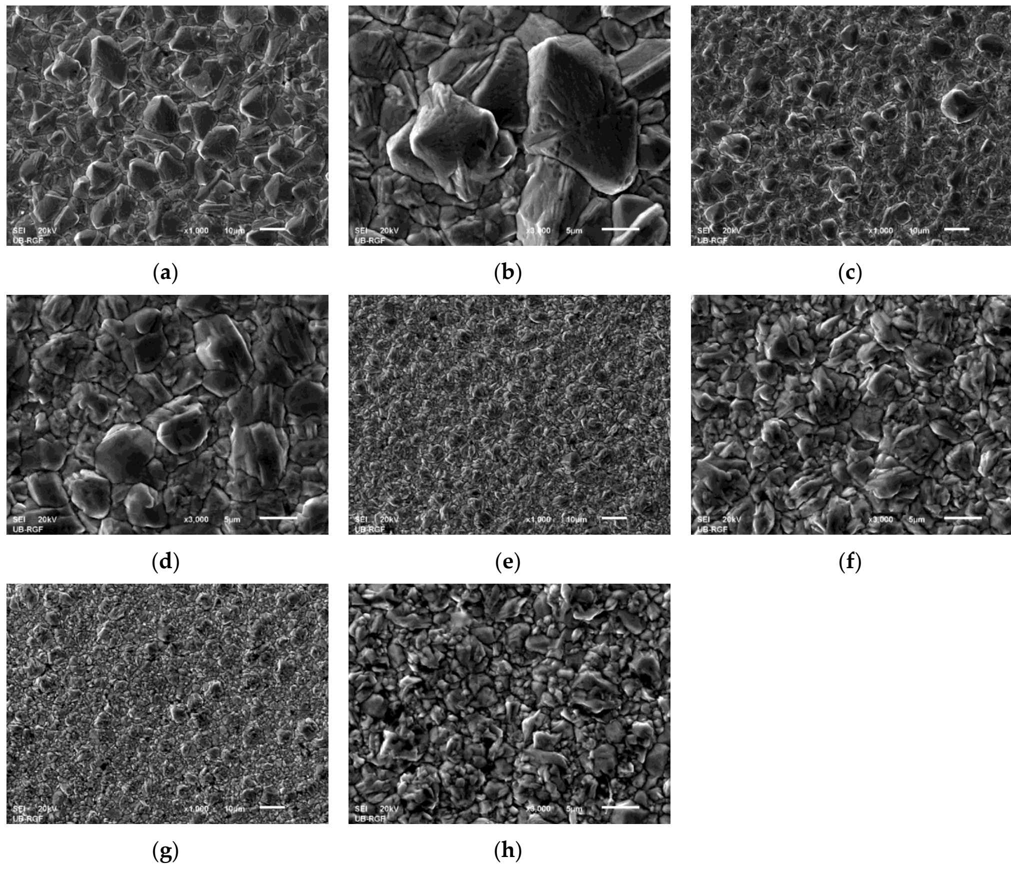

Figure 2. Morphologies of Cu coatings obtained by the PC regimes: (**a**,**b**) 30 Hz (t_p = 28.3 ms), (**c**,**d**) 50 Hz (t_p = 15 ms), (**e**,**f**) 80 Hz (t_p = 7.5 ms), (**g**,**h**) 100 Hz (t_p = 5 ms). In all experiments: j_A = 100 mA·cm^{-2}, and t_c = 5 ms. Magnifications: (**a**,**c**,**e**,**g**) ×1000; (**b**,**d**,**f**,**h**) ×3000.

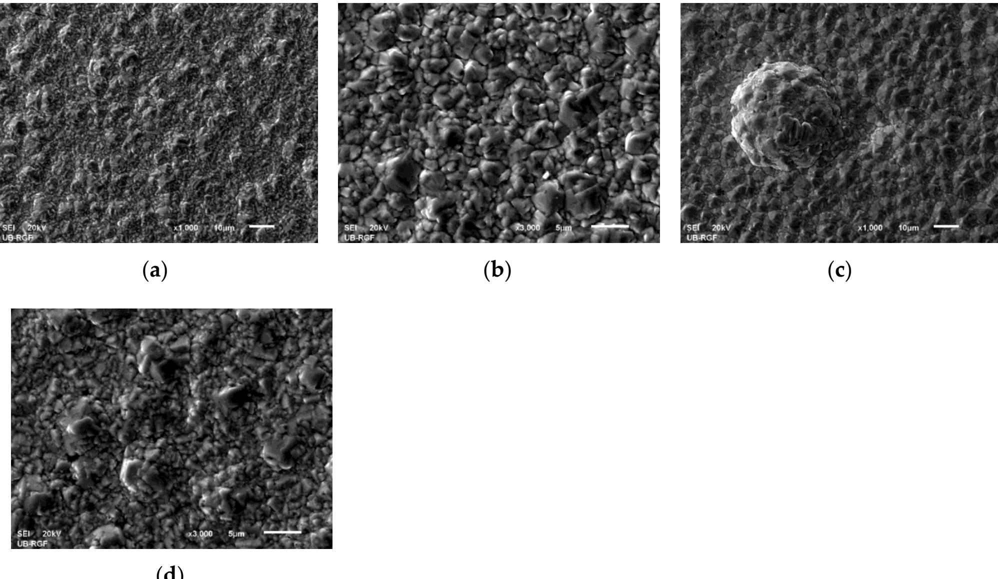

Figure 3. Morphologies of Cu coatings obtained by the PC regimes: (**a**,**b**) j_A = 120 mA·cm^{-2}, and (**c**,**d**) j_A = 140 mA·cm^{-2}. In all experiments: t_c = 5 ms; t_p = 5 ms, ν = 100 Hz. Magnifications: (**a**,**c**) ×1000; (**b**,**d**) ×3000.

At first sight, it can be mentioned that the Cu coating obtained with the amplitude of the current density of 120 mA·cm^{-2} (Figure 3a,b) was relatively similar to that obtained with the amplitude of the

current density of 100 mA·cm^{-2} (Figure 2g,h). A uniform and compact structure with a Cu crystal size of about 5 μm and less were obtained. A completely different surface morphology of Cu was obtained with the amplitude of the current density of 140 mA·cm^{-2} (Figure 3c,d). Aside from parts with relatively uniform surface areas, the globules with a diameter of about 30 μm were also formed by this PC regime.

3.3. X-ray Diffraction (XRD) Analysis of the Produced Cu Coatings

The X-ray diffraction patterns of Cu coatings obtained with the frequencies of 30, 50, 80 and 100 Hz are presented in Figure 4, while those obtained with the current density amplitudes of 100, 120 and 140 mA·cm^{-2} are presented in Figure 5.

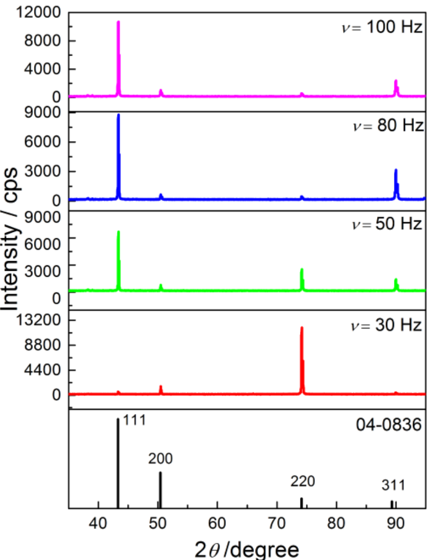

Figure 4. The XRD patterns of Cu coatings obtained by the PC regimes at frequencies of 30, 50, 80 and 100 Hz, and Cu standard (04-0836).

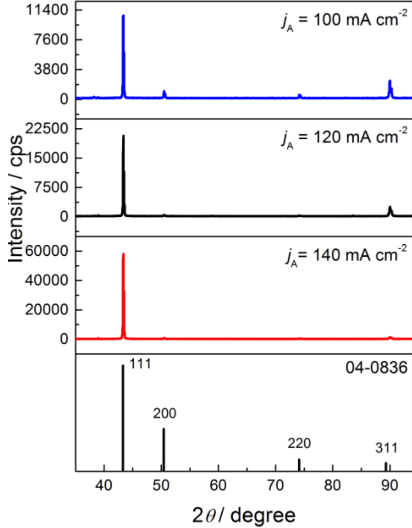

Figure 5. The XRD patterns of Cu coatings obtained by the PC regimes with applied amplitudes of the current density of 100, 120 and 140 mA·cm^{-2}, and Cu standard (04-0836).

Please note that the XRD pattern obtained with the current density amplitude of 100 mA·cm^{-2} (Figure 5) is given again and corresponds to that obtained with a frequency of 100 Hz in Figure 4.

The XRD maximum obtained at 2θ angles of 43.3°, 50.4°, 74.1° and 89.9° belong to the (111), (200), (220) and (311) crystal planes, confirming the face-centered cubic (FCC) crystal lattice of Cu [41]. Aside from the Cu coating obtained at a frequency of 30 Hz, in all other XRD patterns, Cu crystallites were predominantly oriented in the (111) plane. In the XRD pattern of the Cu coating electrodeposited with a frequency of 30 Hz, the predominant orientation of Cu crystallites in the (220) crystal plane was observed. The preferred orientation of Cu coatings was estimated by determination of the "Texture Coefficient" (*TC*(*hkl*)) and "Relative Texture Coefficient" (*RTC*(*hkl*)) [40,41]. It is necessary to note that the *TC*(*hkl*) values larger than 1.00 indicate the existence of the preferred orientation in the (*hkl*) plane. Simultaneously, since four reflections in the 2θ range between 30° and 95° were recorded, the values of *RTC*(*hkl*) coefficients larger than 25% indicate the existence of the preferred orientation [40,41].

The values of *TC*(*hkl*) and *RTC*(*hkl*) coefficients obtained for Cu coatings produced with frequencies of 30, 50, 80 and 100 Hz are given in Tables 2 and 3, respectively.

Table 2. Texture calculations for Cu coatings obtained by the PC regimes at frequencies of 30 and 50 Hz; s—Cu standard.

Plane	*R* (in %)		R_s	*TC*		*RTC* (in %)	
(*hkl*)	$R_{30\ Hz}$	$R_{50\ Hz}$	(in %)	$TC_{30\ Hz}$	$TC_{50\ Hz}$	$RTC_{30\ Hz}$	$RTC_{50\ Hz}$
(111)	4.0	58.6	54.6	0.073	1.07	0.88	22.8
(200)	11.2	6.9	25.1	0.45	0.27	5.4	5.8
(220)	81.9	22.2	10.9	7.5	2.04	90	43.5
(311)	2.9	12.3	9.4	0.31	1.31	3.72	27.9

Table 3. Texture calculations for Cu coatings obtained by the PC regimes at frequencies of 80 and 100 Hz; s—Cu standard.

Plane	*R* (in %)		R_s	*TC*		*RTC* (in %)	
(*hkl*)	$R_{80\ Hz}$	$R_{100\ Hz}$	(in %)	$TC_{80\ Hz}$	$TC_{100\ Hz}$	$RTC_{80\ Hz}$	$RTC_{100\ Hz}$
(111)	67.3	72.7	54.6	1.23	1.33	28.2	35.9
(200)	5.0	7.1	25.1	0.20	0.28	4.6	7.6
(220)	3.6	4.0	10.9	0.33	0.37	7.6	10
(311)	24.1	16.2	9.4	2.6	1.72	59.6	46.5

From Table 2, it can be seen that the Cu coating obtained with a frequency of 30 Hz possesses the strong (220) preferred orientation. According to the same table, the Cu coating obtained at a frequency of 50 Hz showed a (220) preferred orientation with considerably larger ratios of Cu crystallites oriented in the (111) and (311) planes than in the XRD pattern obtained at 30 Hz.

The Cu coatings obtained at frequencies of 80 and 100 Hz showed (311) and (111) preferred orientations (Table 3). Analysis of *TC* and *RTC* coefficients indicated larger ratios of Cu crystallites oriented in the (311) plane than in the (111) plane. Simultaneously, increasing the applied frequency from 80 to 100 Hz led to a decrease of Cu crystallites oriented in the (311) plane and an increase of those oriented in the (111) plane. As indicated in Table 1, the increase in frequency from 30 to 100 Hz is a result of the increase in the average current density from 15 to 50 mA·cm^{-2}.

The *TC*(*hkl*) and *RTC*(*hkl*) coefficients calculated for the Cu coatings obtained with a j_A of 120 and 140 mA·cm^{-2} are given in Table 4.

Similar to the Cu coating obtained with an amplitude of 100 mA·cm^{-2} (100 Hz), the copper coating obtained with an amplitude of 120 mA·cm^{-2} showed (111) and (311) preferred orientations, with the further decrease of ratios of Cu crystallites oriented in the (311) plane and the increase of ratios of Cu crystallites oriented in the (111) plane. Finally, the strong (111) preferred orientation was observed in the Cu coating obtained with an amplitude of 140 mA·cm^{-2}.

Anyway, it follows that increasing the average current density of the electrodeposition from 15 to 70 mA·cm^{-2} led to the strong change in the structure of coatings from the strong (220) to the strong (111) preferred orientation, and it will be explained later in Section 4.

Table 4. Texture calculations for Cu coatings obtained by the PC regimes with a j_A of 120 and 140 mA·cm^{-2}; s—Cu standard.

Plane (*hkl*)	*R* (in %)		R_s (in %)	*TC*		*RTC* (in %)	
	R_{120}	R_{140}		TC_{120}	TC_{140}	RTC_{120}	RTC_{140}
(111)	86.1	95.8	54.6	1.58	1.75	54.3	83.3
(200)	2.0	1.26	25.1	0.080	0.050	2.7	2.4
(220)	1.3	0.76	10.9	0.12	0.070	4.1	3.3
(311)	10.6	2.18	9.4	1.13	0.23	38.9	11.0

3.4. The Roughness Analysis of the Cu Coatings

The AFM surface areas of Cu coatings produced at different frequencies and their line section analyses are shown in Figure 6.

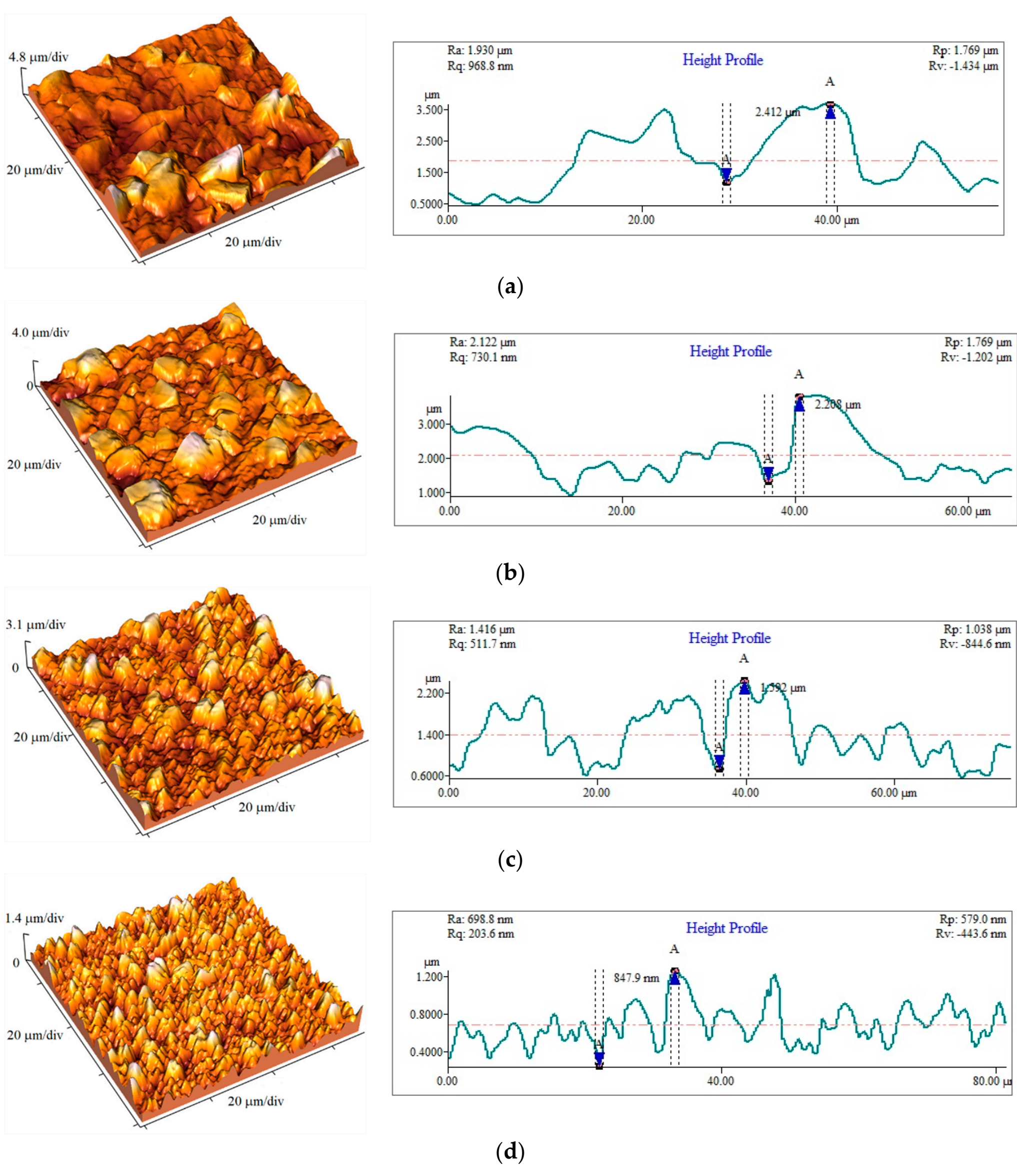

Figure 6. The AFM images and the corresponding line section analyses of Cu coatings obtained by the PC regimes: (**a**) 30 Hz (t_p = 28.3 ms), (**b**) 50 Hz (t_p = 15 ms), (**c**) 80 Hz (t_p = 7.5 ms) and (**d**) 100 Hz (t_p = 5 ms). In all experiments: j_A = 100 mA cm^{-2}, and t_c = 5 ms. Thickness of coatings: δ = 40 µm. Scan area: 70 × 70 µm^2.

The corresponding values of the arithmetic average of the absolute (R_a) roughness obtained by application of the AFM software are given in Table 5. The decrease of roughness by increasing the frequency is clearly visible from Figure 6 and Table 5. This decrease was about three times with the change of frequency from 30 to 100 Hz.

Table 5. The values of R_a roughness obtained by the PC regimes under different electrodeposition conditions; δ—the thickness of coating.

Number of Samples	j_{av}/mA·cm^{-2}	ν/Hz	j_A/mA cm^{-2}	δ/µm	R_a/nm
1	50	100	100	40	169.9
2	40	80	100	40	385
3	25	50	100	40	470.5
4	15	30	100	40	507.3
5	60	100	120	40	237
6	70	100	140	40	229.1
7	50	100	100	10	52.42
8	50	100	100	20	101.5
9	50	100	100	60	286.3

Figure 7 shows the AFM surface areas of the Cu coatings and their line section analyses obtained with a j_A of 120 and 140 mA·cm^{-2}.

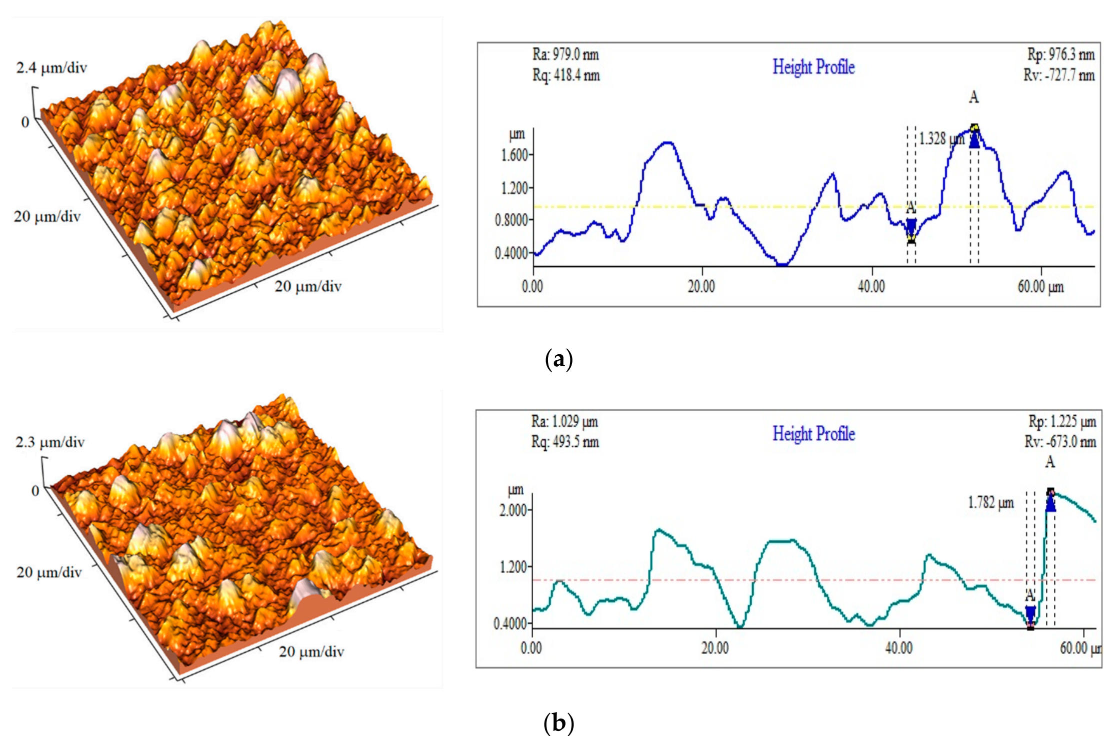

Figure 7. The AFM images and the corresponding line section analyses of Cu coatings obtained by the PC regimes: (**a**) j_A = 120 mA cm^{-2}, and (**b**) j_A = 140 mA cm^{-2}. In all experiments: t_c = 5 ms; t_p = 5 ms, ν = 100 Hz. Thickness of coatings: δ = 40 µm. Scan area: 70 × 70 µm^2.

The R_a values of these Cu coatings are added to Table 5. The surface topographies of the shown AFM images were similar to those obtained with a j_A of 100 mA·cm^{-2} (Figure 6d), while their R_a values were slightly higher than the value obtained with a j_A of 100 mA·cm^{-2}. Please note that analysis of the part of the surface area among globules in the Cu coating obtained with a j_A of 140 mA·cm^{-2} was performed. This is the reason for the similarity of its surface topography and R_a value with those obtained with a j_A of 100 and 120 mA·cm^{-2}. For a comprehensive analysis of the effect of the

parameters of PC regimes on the formation of uniform and compact Cu coatings, the presence of globules (Figure 3c) must not be excluded.

The morphology of metal deposits is primarily determined by either condition of electrolysis, such as type and composition of electrolytes, temperature, stirring of electrolyte, the type of cathode material, the presence of additives to electroplating bath, etc., or parameters defining periodically changing regimes of electrolysis [43], while the effect of the time of electrolysis (i.e., the thickness of the coating) on the morphology of coatings is less pronounced. However, it is well known that the value of the microhardness of coatings strongly depends on its thickness. For that reason, the Cu coating which had a fine-grained structure (Figure 2g,h) and showed minimal roughness (Figure 6d; Table 5), obtained with a j_A of 100 mA·cm^{-2} at 100 Hz, was additionally analyzed by varying its thickness. The AFM surface areas and the corresponding line section analyses of the Cu coatings produced under the given conditions with thicknesses of 10, 20 and 60 μm are shown in Figure 8, while the values of R_a roughness are added to Table 5. The increase of roughness by increasing the thickness of coatings is clearly visible from Figure 8 and Table 5.

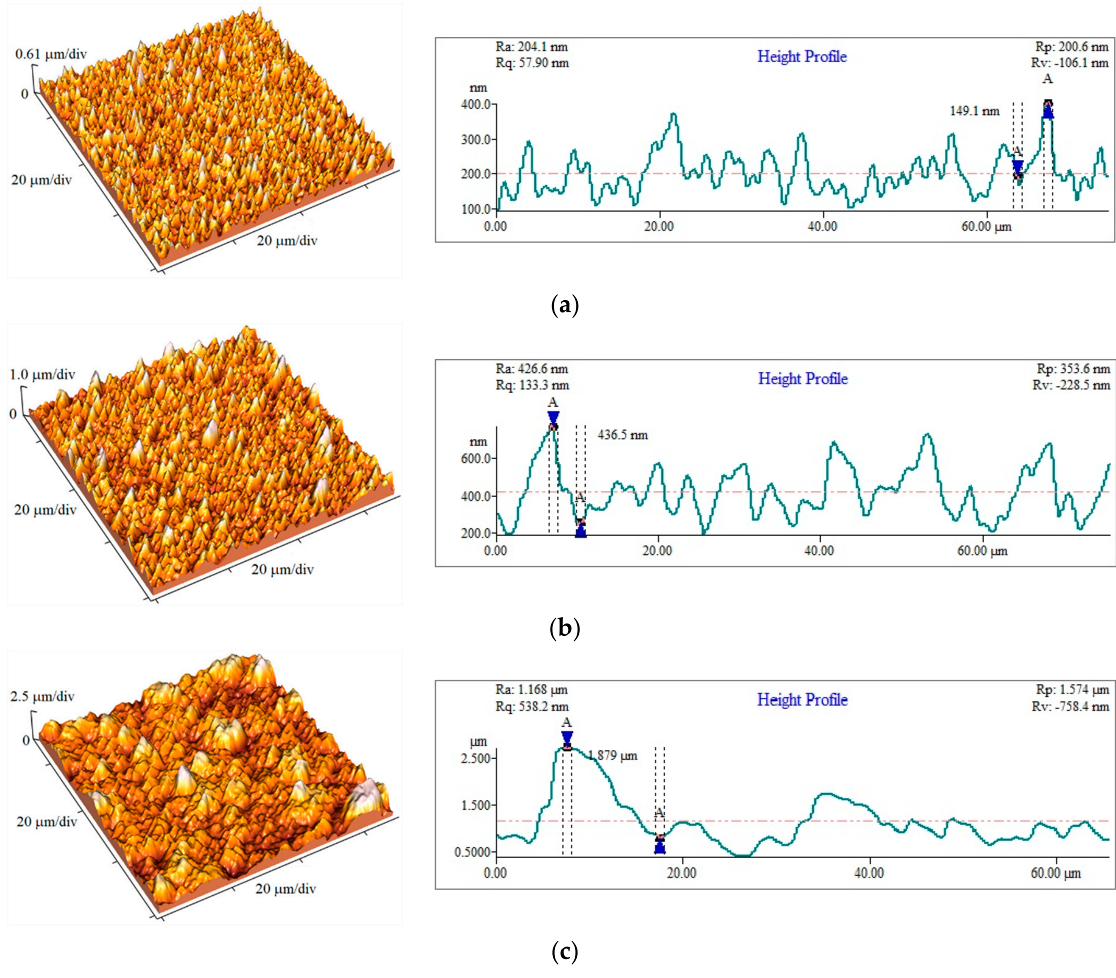

Figure 8. The AFM images and the corresponding line section analyses of Cu coatings obtained by the PC regimes: (**a**) δ = 10 μm, (**b**) δ = 20 μm and (**c**) δ = 60 μm. In all experiments: j_A = 100 mA·cm^{-2}, t_c = 5 ms; t_p = 5 ms, ν = 100 Hz. Scan area: 70 × 70 μm^2.

3.5. Microhardness

3.5.1. Absolute Hardness of the Substrate

Microhardness testing was performed first on the substrate of Si(111) covered with the adhesion and nucleation layers of Cr/Au (30/100 nm) in order to observe their hardness response and to determine the absolute hardness of the substrate. Due to the brittleness of Si, it was not possible to apply all the mentioned loads, but measurements in the load range from 0.245 N to 0.98 N were acceptable for diagonal readings. Based on the Proportional Specimen Resistance (PSR) model [44] and Equation (2) from Appendix A, the hardness of the substrate which is load-independent was obtained. This is shown in Figure 9. The calculated absolute hardness of the substrate was 7.42 GPa.

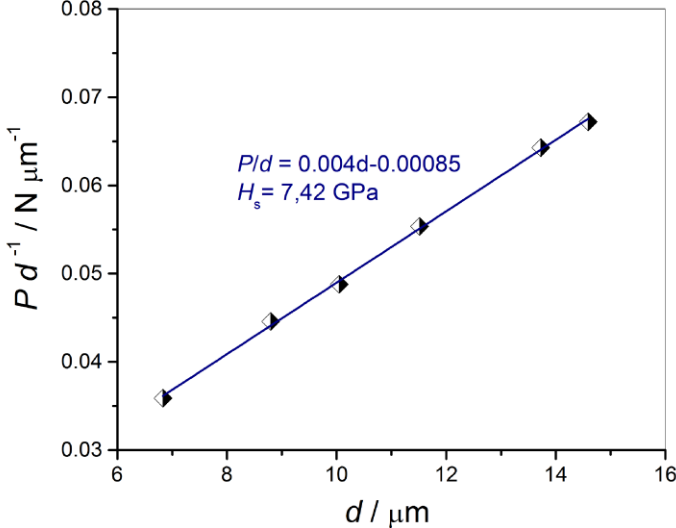

Figure 9. Proportional Specimen Resistance (PSR) plot of applied load through indent diagonal size, *P/d*, versus indent size, *d*, for the Si/Cr/Au substrate.

3.5.2. The Composite and the Coating Hardness

The copper coatings on Si substrates can be considered as a “soft film on a hard substrate” type of composite system [24,45]. Composite and coating hardness values obtained at different frequencies, different amplitudes of the current density and different coating thicknesses were measured and calculated. Changes in the microstructure of the coating will directly affect the values of composite hardness and coating microhardness.

When analyzing the hardness of the composite systems, three areas can be distinguished according to the value of the relative indentation depth (RID = h/δ), where h is the indentation depth and δ is the total coating thickness. When the RID is between 0 and 0.1, it is considered that the influence of coating hardness on composite hardness value is dominant [46]. For the relative indentation depths between 0.1 and 1, it was found that the hardness of the composite system depends on both the hardness of the substrate and the coating hardness and their relative difference. The influence of the substrate is dominant for the values of the RID ≥ 1.

The effect of changing the frequency on the composite hardness H_c, and coating microhardness H_{coat}, is shown in Figure 10a,b, respectively.

As already mentioned, in this set of experiments, the current density amplitude was maintained at 100 mA cm^{-2} and the thickness of the coatings was 40 µm. An increase in frequency led to an increase in the composite hardness of the system. The values of the coating microhardness were calculated according to the C–L model. The highest values of the composite hardness and the coating microhardness were obtained at a frequency of 100 Hz and the lowest values were obtained for a frequency of 30 Hz. The influence of frequency on the microstructure of the coatings and its hardness

is best observed for the relative indentation depth between 0 and 0.1, when the influence of the coating on the composite hardness is dominant.

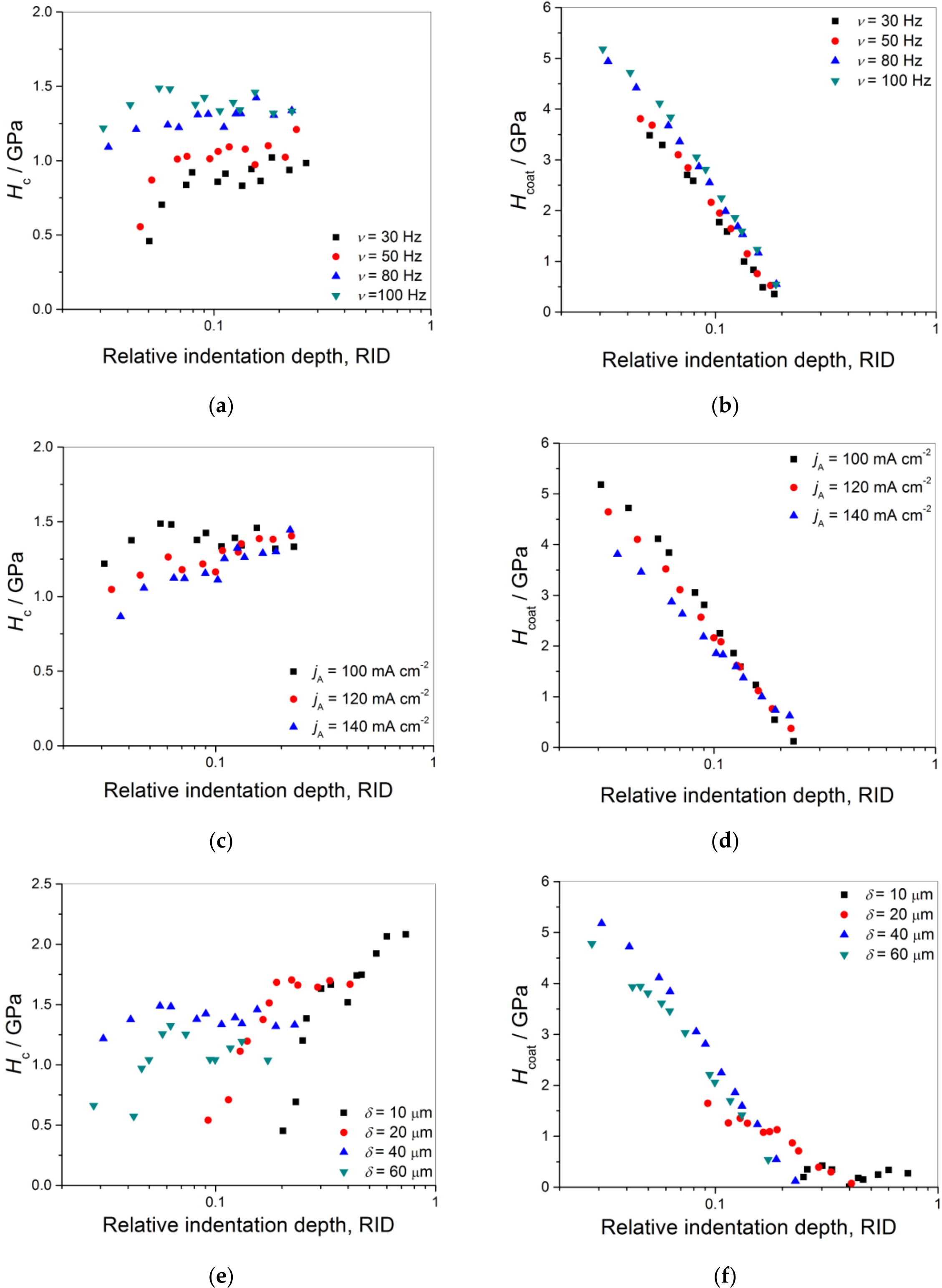

Figure 10. The hardness variation with relative indentation depth calculated according to the Chicot–Lesage composite hardness model: (**a**,**c**,**e**) composite systems (H_c), and (**b**,**d**,**f**) the microhardness of Cu coatings (H_{coat}): (**a**,**b**) ν: 30, 50, 80 and 100 Hz, (**c**,**d**) j_A: 100, 120 and 140 mA·cm^{-2}, (**e**,**f**) δ: 10, 20, 40 and 60 µm.

Variations of the composite hardness and coating microhardness with the current density amplitudes are shown in Figure 10c,d. The frequency value was maintained at 100 Hz and the thickness of the coatings was 40 μm. Three values of the current density amplitude were selected for analysis: 100, 120 and 140 mA·cm^{-2}. Please note that values obtained with a j_A of 100 mA·cm^{-2} are repeated and they correspond to those given in Figure 10a,b for 100 Hz. The maximum value of the composite hardness was obtained for the copper coating deposited with the current density amplitude of 100 mA·cm^{-2} and the minimum value for the amplitude of 140 mA·cm^{-2} (Figure 10c). The results of the calculated coating microhardness according to the C–L model more clearly indicate the influence of the amplitude change on the microstructure and the hardness of the coating, and the highest coating microhardness value was obtained for the current density amplitude value of 100 mA·cm^{-2} (Figure 10d).

Coating thickness is a parameter that significantly affects the composite hardness. As the thickness increases, the coating's participation in the composite system increases. Variations of the composite hardness and coating microhardness with the thickness of coatings at optimal deposition parameters (ν = 100 Hz and j_A = 100 mA·cm^{-2}) are given in Figure 10e,f. Please note that values given for a thickness of 40 μm are already given in Figure 10a–d. The coating thicknesses of 10, 20, 40 and 60 μm were chosen. The calculated values of coating microhardness according to the C–L model are given in Figure 10f. At the optimum deposition parameters, the highest value of composite hardness was obtained for a coating thickness of 40 μm.

4. Discussion

It is clear from the above consideration that the highest value of copper coating microhardness was achieved with a j_A of 100 mA·cm^{-2} at 100 Hz, i.e., and with a j_{av} of 50 mA·cm^{-2} (Figure 2g,h). This coating was fine-grained and had the smallest roughness. High coating microhardness values were also achieved at a frequency of 80 Hz (Figure 2e,f), as well as with the current density amplitude j_A of 120 mA·cm^{-2} (Figure 3a,b). These coatings also have fine-grained structure and their roughness was slightly higher than that obtained with a j_A of 100 mA·cm^{-2} at 100 Hz.

For the lowest frequency value of 30 Hz, the obtained coating was coarse-grained with large relatively well-defined grains (Figure 2a,b). The roughness of this coating was considerably higher than those observed at 80 and 100 Hz, as well as with a j_A of 120 mA·cm^{-2}. The direct consequence is the lower coating microhardness value. Similar results to those for 30 Hz were obtained when the 50 Hz frequency was applied (Figure 2c,d). Applying the current density amplitude of 140 mA·cm^{-2}, a rough structure with globules was obtained (Figure 3c,d), and as a result of this, the decrease of microhardness of this Cu coating was observed.

All the above-mentioned surface morphologies had a thickness of 40 μm. In coatings of 10 and 20 μm thickness, a contribution of the substrate hardness to the composite hardness was significant. With an increasing thickness of the coatings, the roughness of coatings increased (Figure 8), resulting in a decrease of composite hardness and coating microhardness for the coating electrodeposited with a thickness of 60 μm relative to that of 40 μm.

Due to the strong dependence of morphology and structure of Cu coatings on the microhardness, optimization of the process of the formation of Cu coatings with a compact and uniform structure on Si(111) by the PC regime was done and discussed as follows.

Table 6 shows summarized values of overpotential amplitude (η_A) response obtained with analyzed parameters of the PC regime during electrodeposition processes.

Table 6. Overpotential amplitude (η_A) responses obtained during electrodeposition processes with the selected parameters of the PC regimes.

The PC Regime	ν/Hz				j_A/mA·cm^{-2}	
	30	**50**	**80**	**100**	**120**	**140**
η_A/mV	99–135	135–200	210–290	290–350	320–425	380–500

In the PC regimes, overpotential amplitude responses consist of the activation and diffusion parts, where a contribution of the activation part of the overpotential depends on the pause-to-pulse ratio and increases with it, i.e., a contribution of the activation part increases with an increase of pause duration and a decrease of frequency [47]. The set of equations explaining it is given in Appendix C.

Regarding the fact the that formation of large well-defined grains is a characteristic of the activation control of the electrodeposition [38,43], it is clear that Cu coatings obtained with a p of 5.66 and 3 (30 and 50 Hz; Figure 2a–d) are formed under conditions of the dominant activation control of the electrodeposition. Of course, a contribution of the activation control to the overall control was larger with an applied frequency of 30 Hz (Figure 2a,b) than with 50 Hz (Figure 2c,d). The high contribution of the activation control at 30 Hz is confirmed by an overpotential amplitude response at this frequency of 99−135 mV (Table 6), which corresponds to the end of the activation control and to the beginning of the mixed activation–diffusion control of the electrodeposition (Figure 1).

The formation of globules with an amplitude of 140 mA·cm^{-2} (Figure 3c) clearly indicates that the contribution of diffusion becomes dominant in the overall control of the electrodeposition process. This is confirmed by an overpotential amplitude response of 380–500 mV corresponding to the end of the mixed activation–diffusion control (Figure 1).

Hence, optimum conditions for the formation of compact and uniform films of satisfactory microhardness corresponds to the range of overpotential in the mixed activation–diffusion control between the end of the effect of the activation control and the beginning of the dominant effect of diffusion control. For these working conditions, the optimum conditions are in the range of overpotentials between 200 and 400 mV (denoted by vertical dash lines in Figure 1), and they can be achieved in different ways by appropriate selection of parameters of the PC regimes. Of course, one challenge in the future will be to extend this overpotential range.

Aside from the strong effect on the morphology of the Cu coatings, the applied parameters of PC regimes also had a strong effect on the structure of the coatings leading to a change of preferred orientation from the strong (220) to the strong (111), that can be explained in the following way.

For the FCC crystal lattice of Cu, the values of surface energy of crystal planes follow the trend: $\gamma_{111} < \gamma_{100} < \gamma_{311} < \gamma_{110}$ [48,49]. As a result of different surface energy values, rate of electrodeposition is different on crystal planes, following the opposite trend from that for surface energy values [50]. The (100), (110) and (311) crystal planes are situated to the group of fast-growing planes, while the (111) plane belongs to the group of slow-growing crystal planes [51]. It means that during the electrodeposition process, the fast-growing (100), (110) and (311) planes disappear firstly, while the slow-growing (111) plane survives.

The average current density of 15 mA·cm^{-2} is too low to cause the disappearance of the fast-growing (220) plane, and the coarse Cu coating with large grains obtained at this average current density (i.e., at 30 Hz) showed the strong (220) preferred orientation. Intensification of the electrodeposition process through an increase of j_{av} from 15 to 25 mA·cm^{-2} led to faster disappearing of Cu crystallites oriented in the (220) plane, and an increase of the ratios of Cu crystallites oriented in the next (311) plane. As a result of this, the Cu coating obtained at a j_{av} of 25 mA·cm^{-2} (i.e., at 50 Hz) showed a smaller degree of (220) preferred orientation than that obtained at 30 Hz. The further increase of the average current density from 40 mA cm^{-2} (80 Hz) and 50 mA·cm^{-2} (100 Hz) to 60·mA·cm^{-2} (j_A = 120 mA·m^{-2}) led to the formation of Cu coatings with crystallites preferentially oriented in the (311) and (111) planes. It is necessary to note that the ratio of Cu crystallites oriented in the fast-growing (311) plane decreased, while the ratio of Cu crystallites oriented in the slow-growing (111) plane increased by increasing the average current density from 40 to 60 mA cm^{-2}. Finally, the Cu coating obtained at the average current density of 70 mA·cm^{-2} at which diffusion became the dominant process possessed the strong (111) preferred orientation.

Composite hardness values, H_c, were calculated from the experimentally measured indentation diagonals according to Equation (1) from Appendix A. The increase of H_c for the RID < 0.1 can be explained by strengthening of the coatings by deformation [35,36,52].

The obtained results are in accordance with the Hall−Petch effect [53], predicting the linear dependence of the hardness of the deposits on the reciprocal square root of grain size [54,55]. Namely, it is well known that an increase in the current density of electrodeposition leads to a decrease of grain size causing an increase in the hardness of deposits [53]. This linear dependence is valid up to some value of grain size corresponding to the certain current density, after which the value of the hardness of the deposit begins to decrease. The decrease of hardness after maximum value, i.e., the transition from grain-size strengthening to grain-size softening can be attributed to a change in the triple junction (i.e., intersection of three or more grain boundaries) volume fraction [53]. In our case, it is clear that the increase of hardness with the decrease of grain size can be attributed to the grain-size strengthening effect achieved in the mixed activation–diffusion control, while the grain size softening effect corresponds to the beginning of the dominant diffusion control of electrodeposition when globules forms.

According to the C–L model, it is possible to calculate the hardness of the coating only from the microhardness results (diagonal of the indent), because the values obtained for the coating hardness are influenced by the applied load. How the coating hardness changes according to this model will depend not only on the type of composite system, but also on the hardness of the coating and the substrate and the ratio of their hardness values. Due to the observation of the variation in hardness of the coating with RID, we applied the model to all samples. According to Equation (7) (Appendix A), the largest effects on the coating hardness have coefficients A, B, and C, which are dependent on parameter f. This parameter is a function of δ/d, and the C–L model gives the most reliable results for the δ/d ratios of about 1 [56,57]. In our case, this condition is fulfilled for coating thicknesses of 10 and 20 μm in the whole range of examined loads. For the coating thickness of 40 μm, this condition is fulfilled in the RID range between 0.1 and 1 for the composite hardness and to a greater extent for the coating hardness. Regarding the coating thickness of 60 μm, the δ/d ratio is considerably larger than 1, causing noticeably larger values for the composite and the coating hardness. It is worth noting that such high values of coating hardness have been reported already for the Cu coatings obtained by pulse electrodeposition [52].

The discrepancy between the composite hardness and the calculated coating hardness can be explained as follows: the composite hardness is determined from Equation (1), while the coating hardness is determined from Equation (7) (both equations from Appendix A). As already mentioned, the main parameter affecting the coating hardness is δ/d, where a contribution of this parameter in the calculation of the coating hardness increases by increasing the thickness of the coating. As a result of this, the difference between the composite and the coating hardness increases by increasing the coating thickness, causing a limitation in the application of the C–L model for the thicker coatings. Of course, morphological characteristics of coatings, such as shape and size of grains, roughness of the coatings, as well as substrate type, also affect the final values of the composite and the coating hardness.

Anyway, the high microhardness showed the Cu coatings with Cu crystallites predominantly oriented in the (111) plane, which is the closest-packed crystal plane of the FCC lattice. According to our opinion, similar to mirror bright Cu coatings [58], the (111) plane is not crucial for the enhanced microhardness of coatings, but it plays a significant role in this mechanical characteristic of Cu coatings.

5. Conclusions

The conditions enabling the formation of compact and uniform Cu coatings of a high microhardness by the regime of pulsating current (PC) were defined. The Cu coatings were produced in the 15−70 mA·cm^{-2} range by varying either the frequency (pause duration) or the current density amplitude. The maximal microhardness showed the Cu coating obtained at a frequency of 100 Hz with the current density amplitude of 100 mA·cm^{-2} and a pause duration of 5 ms. The optimal thickness of the coating was 40 μm.

It was shown the strong dependence of the microhardness of coatings on their morphology and topography. The copper coating with maximal microhardness was fine-grained and showed low

roughness. The coatings with large and relatively well-defined Cu crystals and globules had a smaller microhardness from those with the fine-grained structure. Analysis of the overpotential amplitude responses showed that the Cu coatings of the highest microhardness are obtained in the range of overpotentials between the end of the effect of the activation control and the beginning of the dominant effect of diffusion control of electrodeposition.

Aside from the strong influence on morphology, and hence on microhardness of the Cu coatings, parameters of the PC regimes also affect their crystal structure. The preferred orientation of the coatings changed from the strong (220) to the strong (111) preferred orientation by increasing the average current density. This change was caused by the dependence of the rate of electrodeposition on the process parameters, i.e., on selected average current density.

The Chicot–Lesage (C–L) model was applied for a determination of the coating hardness. The most reliable values for the coating hardness are obtained for the thicknesses of coatings from 10 and 20 µm. For the coating thickness from 40 µm, the reliable values are obtained in the RID range between 0.1 and 1. Finally, for the coating thickness of 60 µm, the considerably higher values of coating hardness, but in accordance with those found in the literature, were obtained, making this model less appropriate for thicker coatings of copper. The limitations in the application of the C–L model for the thicker coatings of copper are also discussed.

Author Contributions: I.O.M. performed experiments and contributed in analysis of microhardness; J.S.L. performed analysis of microhardness; D.G.V.R. performed the AFM analysis; R.V. performed the XRD analysis; V.J.R. contributed in discussion of microhardness measurement; and N.D.N. conceived and wrote the paper. All authors have read and agreed to the published version of the manuscript.

Funding: This research received no external funding.

Acknowledgments: This work was funded by the Ministry of Education, Science and Technological Development of the Republic of Serbia.

Conflicts of Interest: The authors declare no conflict of interest.

Appendix A

Appendix A.1. Theory of the Composite Hardness Model

The model suggested by Chicot and al. [27,35] is based on the analogy between the variation of Young's modulus of reinforced composites in the function of the volume fraction of particles and the variation of the composite hardness with the indentation load. The values of the composite hardness are in the range between the hardness of the substrate and the hardness of the film [35,36,56,57,59,60]. The model assumes the use of only those data that can be obtained from micro-indentation tests (measured composite hardness, H_c).

The composite hardness value depends on the measured diagonal size and applied load and it is defined by Equation (A1) [56,57,59]:

$$H_c = \frac{1.8544 \cdot P}{d^2} \quad \text{(A1)}$$

where P is the applied load (in N), the constant 1.8544 is a geometrical factor for the Vickers pyramid and d is the average diagonal length of the indent (in m). In order to apply a composite hardness model, it is necessary to know the absolute hardness of the substrate before depositing the coating.

The Proportional Specimen Resistance model (PSR) of Li and Bradt [44] is suitable for analyzing the variation of substrate microhardness with the load:

$$P = a_1 \cdot d + \frac{P_c}{d_0^2} \cdot d^2 \quad \text{(A2)}$$

Here, P_c is the critical applied load above which microhardness becomes load-independent and d_0 is the corresponding diagonal length of the indents. A plot of P/d against d will give a linear plot.

The slope value multiplied by the geometric constant gives the value of the absolute hardness of the substrate (H_S).

The measured composite hardness values of the system are not constant because the hardness is load-dependent. Meyer's law [61] expresses the variation of the diagonal size in the function of the applied load. Meyer's law can be expressed as the relation:

$$P = a^* \cdot d^{n*} \tag{A3}$$

The variation of the hardness value with load is presented by the factor n*, characterizing the way of change of the load hardness, as presented by the Equation (A4) [56,57,59]:

$$F\left(\frac{\delta}{d}\right) = \left(\frac{\delta}{d}\right)^m = f \quad \text{where} \quad m = \frac{1}{n^*} \tag{A4}$$

where δ is the coating thickness, d is average indent diagonal size, and exponent m corresponds to the inverse of Meyer index for composite material. The value of m (composite Mayer's index) is calculated by a linear regression performed on all experimental points for a given film-substrate system as:

$$Lnd = m \cdot LnP + b \tag{A5}$$

Then, the composite hardness model can be expressed by Equation (A6) [56,57]:

$$H_c = (1-f)/\left(\frac{1}{H_S} + f \cdot \left(\frac{1}{H_{coat}} - \frac{1}{H_S}\right)\right) + f \cdot (H_S + f \cdot (H_{coat} - H_S)) \tag{A6}$$

Rewriting this relation as a polynomial in terms of H_{coat}, the coating hardness can be calculated which is thus the positive root of the equation:

$$\begin{aligned} & A \cdot H_{coat}^2 + B \cdot H_{coat} + C = 0 \\ & A = f^2 \cdot (f-1) \\ & B = \left(-2 \cdot f^3 + 2 \cdot f^2 - 1\right) \cdot H_S + (1-f) \cdot H_c \\ & C = f \cdot H_c \cdot H_S + f^2 \cdot (f-1) \cdot H_S^2 \end{aligned} \tag{A7}$$

The parameters A, B and C represent the coefficients of the second-order polynomials in Equation (A7) and the hardness of the coatings is the positive root of this equation. The parameter $(\delta/d)^m$, or function f, can be calculated from Equation (A4), and Meyer's index from Equation (A5). With the known value of m, only the hardness of the coatings remains to calculate.

Appendix B

Determination of the "Texture Coefficient", $TC(hkl)$ and the "Relative Texture Coefficient", $RTC(hkl)$ by analysis of the XRD data

The ratio of reflection intensity (hkl) to the sum of all intensities of the recorded reflections, R (hkl), (in %) is given by Equation (A8) [39–41]:

$$R(hkl) = \frac{I(hkl)}{\sum_i^4 I(h_i k_i l_i)} \times 100 \tag{A8}$$

where I (hkl) is the reflection intensity (hkl), in cps, and $\sum_i^4 I(h_i k_i l_i)$ is the sum of all intensities of the recorded reflections, in cps, for the deposit being considered.

The "Texture Coefficient", $TC(hkl)$, for every (hkl) reflection is defined by Equation (A9):

$$TC(hkl) = \frac{R(hkl)}{R_s(hkl)} \tag{A9}$$

where $R_s(hkl)$ is defined in the same way as given by Equation (A9), but is related to the Cu standard (04-0836). This coefficient gives accurate quantitative information about the absolute reflection intensity.

Finally, the "Relative Texture Coefficient", $RTC(hkl)$ is defined by Equation (A10):

$$RTC(hkl) = \frac{TC(hkl)}{\sum_{i}^{4} TC(h_i k_i l_i)} \times 100 \tag{A10}$$

The RTC (hkl) coefficient defines the reflection intensity (hkl) relative to the standard (included in the TC values).

Appendix C

The dependence of the overpotential amplitude on parameters of the pulsating current regimes

In the PC regime, the overpotential amplitude, η_A can be presented by Equation (A11) [47]:

$$\eta_A = \frac{b_c}{2.3} \ln \frac{j_{av}(p+1)}{j_0} + \frac{b_c}{2.3} \ln \frac{1}{1 - \frac{j_{av}}{j_L}} \tag{A11}$$

where b_c is the cathodic Tafel slope, j_L is the limiting diffusion current density, and j_0 is the exchange current density. The activation part of overpotential, η_{act} is given by Equation (A12):

$$\eta act = \frac{b_c}{2.3} \ln \frac{j_{av}}{j_0}(p+1) \tag{A12}$$

while the diffusion part of overpotential, η_{diff} is given by Equation (A13):

$$\eta_{diff} = \frac{b_c}{2.3} \ln \frac{1}{1 - \frac{j_{av}}{j_L}} \tag{A13}$$

Hence, it follows from Equation (A12) that the activation part of the overpotential depends on the pause-to-pulse ratio and increases with it.

Equation (A12) can be rewritten in the form:

$$\eta_A = \eta_{const} + \frac{b_c}{2.3} \ln(p+1) \tag{A14}$$

where η_{const} is the overpotential in the constant regime of electrolysis defined by Equation (A15):

$$\eta_{const} = \frac{b_c}{2.3} \ln \frac{j_{av}}{j_0} + \frac{b_c}{2.3} \ln \frac{1}{1 - \frac{j_{av}}{j_L}} \tag{A15}$$

if $j_{av} = j$, where j is the current density in the constant regime of electrolysis.

From the point of view of the average current density, it means that there is no difference between electrochemical deposition processes in the constant regimes and PC conditions. On the other hand, it is very clear from Equation (A15) that at the fixed value of the average current density the amplitude of overpotential depends on the pause-to-pulse ratio, and it increases with the increasing pause-to-pulse ratio.

According to Popov and Pavlović [62], the degree of diffusion control of electrodeposition process, ω, is defined by Equation (A16):

$$\omega = \frac{\ln \frac{1}{1-\frac{j_{av}}{j_L}}}{\ln \frac{j_{av}}{j_0} + \ln(p+1) + \ln \frac{1}{1-\frac{j_{av}}{j_L}}} \quad \text{(A16)}$$

and it represents a contribution of diffusion overpotential to total cathode overpotential. Hence, due to the increase of the activation part of overpotential with the increasing pause-to-pulse ratio, the degree of diffusion control will decrease with the increasing pause-to-pulse ratio, resulting in the possible change of texture of deposit. It is noteworthy that it is valid if $j_{av} < j_L$ in the mixed controlled deposition.

References

1. Rohan, J.F.; Thompson, D. Frontiers of Cu Electrodeposition and Electroless plating for on-chip Interconnects. In *Copper Electrodeposition for nanofabrication of Electronics Devices*; Kondo, K., Alkolkar, R.N., Barkey, D.P., Yokoi, M., Eds.; Springer: New York, NY, USA, 2014; Volume 171, pp. 99–101. [CrossRef]
2. Pellicer, E.; Varea, A.; Pané, S.; Sivaraman, K.M.; Nelson, B.J; Suriñach, S.; Baró, M.D.; Sort, J. A comparison between fine-grained and nanocrystalline electrodeposited Cu–Ni films Insights on mechanical and corrosion performance. *Surf. Coat. Technol.* **2011**, *205*, 5285–5293. [CrossRef]
3. Banthia, S.; Sengupta, S.; Das, S.; Das, K. Cu, Cu-SiC functionally graded coating for protection against corrosion and wear. *Surf. Coat. Technol.* **2019**, *374*, 833–844. [CrossRef]
4. Banthia, S.; Sengupta, S.; Das, S.; Das, K. Synthesis and characterization of novel Cu, Cu-Si functionally graded coating by pulse reverse electrodeposition. *Appl. Surf. Sci.* **2019**, *467–468*, 567–579. [CrossRef]
5. Gupta, S.K.; Misra, R.D. An experimental investigation on flow boiling heat transfer enhancement using Cu-TiO_2 nanocomposite coating on copper substrate. *Exp. Therm. Fluid Sci.* **2018**, *98*, 406–419. [CrossRef]
6. Gupta, S.K; Misra, R.D. Effect of two-step electrodeposited Cu–TiO2 nanocomposite coating on pool boiling heat transfer performance. *J. Therm. Anal. Calorim.* **2019**, *136*, 1781–1793. [CrossRef]
7. Gupta, S.K.; Misra, R.D. Experimental study of pool boiling heat transfer on copper surfaces with Cu-Al_2O_3 nanocomposite coatings. *Int. Commun. Heat Mass Transf.* **2018**, *97*, 47–55. [CrossRef]
8. Cortés, M.; Martínez, S.; Serre, C.; Gómez, E.; Pérez-Rodríguez, A.; Vallés, E. Design and electrochemical preparation of inductive copper coil for magnetic particles detection. *Sens. Actuators B* **2012**, *173*, 737–744. [CrossRef]
9. Ming, P.M; Zhu, D.; Zeng, Y.B; Hu, Y.Y. Wear resistance of copper EDM tool electrode electroformed from copper sulfate baths and pyrophosphate baths. *Int. J. Adv. Manuf. Technol.* **2010**, *50*, 635–641. [CrossRef]
10. Delbos, E.; Omnès, L.; Etcheberry, A. Bottom-up filling optimization for efficient TSV metallization. *Microelectron. Eng.* **2010**, *87*, 514–516. [CrossRef]
11. Arai, S.; Hasegawa, T.; Kaneko, N. Fabrication of three-dimensional Cu/Ni multilayered microstructure by wet process. *Electrochim. Acta* **2004**, *49*, 945–950. [CrossRef]
12. Ladani, L.; Awad, I.; She, Y.; Dardona, S.; Schmidt, W. Fabrication of Carbon Nanotube/Copper and Carbon Nanofiber/Copper Composites for Microelectronics. *Mater. Today Commun.* **2017**, *11*, 123–131. [CrossRef]
13. Frost, G.; Ladani, L. Development of High-Temperature-Resistant Seed Layer for Electrodeposition of Copper for Microelectronic Applications. *J. Electron. Mater.* **2020**, *49*, 1387–1395. [CrossRef]
14. Marro, J.B.; Darroudi, T.; Okorod, C.A.; Obeng, Y.S.; Richardson, K.C. The influence of pulse plating frequency and duty cycle on the microstructure and stress state of electroplated copper films. *Thin Solid Films* **2017**, *621*, 91–97. [CrossRef] [PubMed]
15. Pasa, A.A.; Schwarzacher, W. Electrodeposition of Thin Films and Multilayers on Silicon. *Phys. Status Solid. A* **1999**, *173*, 73–84. [CrossRef]
16. Kristof, P.; Pritzker, M. Improved Copper Plating Through the Use of Current Pulsing & Ultrasonic Agitation. *Plat. Surf. Finish.* **1999**, *85*, 237–240.
17. Tantavichet, N.; Pritzker, M.D. Effect of plating mode, thiourea and chloride on the morphology of copper deposits produced in acidic sulphate solutions. *Electrochim. Acta* **2005**, *50*, 1849–1861. [CrossRef]

18. Tantavichet, N.; Damronglerda, S.; Chailapakulb, O. Influence of the interaction between chloride and thiourea on copper electrodeposition. *Electrochim. Acta* **2009**, *55*, 240–249. [CrossRef]
19. Baral, A.; Sarangi, C.K.; Tripathy, B.C.; Bhattacharya, I.N.; Subbaiah, T. Copper electrodeposition from sulfate solutions—Effects of selenium. *Hydrometallurgy* **2014**, *146*, 8–14. [CrossRef]
20. Mallik, A.; Ray, B.C. Morphological study of electrodeposited copper under the influence of ultrasound and low temperature. *Thin Solid Films* **2009**, *517*, 6612–6616. [CrossRef]
21. Mallik, A.; Bankoti, A.; Ray, B.C. A study on the modification of Conventional Electrochemical crystallization under sonication: The Phenomena of secondary nucleation. *Electrochem. Solid-State Lett.* **2009**, *12*, F46–F49. [CrossRef]
22. Hakamada, M.; Nakamoto, Y.; Matsumoto, H.; Iwasaki, H.; Chen, Y.; Kusuda, H.; Mabuchi, M. Relationship between hardness and grain size in electrodeposited copper films. *Mater. Sci. Eng. A* **2007**, *457*, 120–126. [CrossRef]
23. Augustin, A.; Huilgol, P.; Udupa, K.R.; Bhat, K.U. Effect of current density during electrodeposition on microstructure and hardness of textured Cu coating in the application of antimicrobial Al touch surface. *J. Mech. Behav. Biomed. Mater.* **2016**, *63*, 352–360. [CrossRef] [PubMed]
24. Ma, Z.S.; Zhou, Y.C.; Long, S.G.; Lu, C. On the intrinsic hardness of a metallic film/substrate system: Indentation size and substrate effects. *Int. J. Plast.* **2012**, *34*, 1–11. [CrossRef]
25. Muller, W.H.; Sbeiti, M.; Worrack, H. The effect of Dwell Time Variation during Microhardness Testing. In Proceedings of the 10th Youth Symposium on Experimental Solid Mechanics, Chemnitz, Germany, 25–28 May 2011.
26. Fuguo, L.; Jinghui, L.; Bo, C.; Chengpeng, W.; Lei, W. Size effects at dwell stage of micro-indentation for pure aluminum. *Rare Met. Mater. Eng.* **2014**, *12*, 2931–2936. [CrossRef]
27. Chicot, D.; Lesage, J. Absolute hardness of films and coatings. *Thin Solid Films* **1995**, *254*, 123–130. [CrossRef]
28. Hong, S.H.; Kim, K.S.; Kim, Y.M.; Hahn, J.H.; Lee, C.S.; Park, J.H. Characterization of elastic moduli of Cu thin films using nanoindentation technique. *Compos. Sci. Technol.* **2005**, *65*, 1401–1408. [CrossRef]
29. Saha, R.; Xue, Z.; Huang, Y.; Nix, W.D. Indentation of a soft metal film on a hard substrate: Strain gradient hardening effects. *J. Mech. Phys. Solids* **2011**, *49*, 1997–2014. [CrossRef]
30. Zong, Z.; Lou, J.; Soboyejo, O.O.; Elmustafa, A.A; Hammada, F.; Soboyejo, W.O. Indentation size effects in the nano- and micro-hardness of fcc single crystal metals. *Mater. Sci. Eng. A* **2006**, *434*, 178–187. [CrossRef]
31. Elmustafa, A.A.; Stone, D.S. Indentation size effect in polycrystalline F.C.C. metals. *Acta Mater.* **2002**, *50*, 3641–3650. [CrossRef]
32. Beegan, D.; Chowdhury, S.; Laugier, M.T. Modification of composite hardness models to incorporate indentation size effects in thin films. *Thin Solid Films* **2008**, *516*, 3813–3817. [CrossRef]
33. Bull, S.J.; Rickerby, D.S. New developments in the modeling of the hardness and scratch adhesion of thin films. *Surf. Coat. Technol.* **1990**, *42*, 149–164. [CrossRef]
34. Burnett, P.J.; Rickerby, D.S. The mechanical properties of wear-resistant coatings. II: Experimental studies and interpretation of hardness. *Thin Solid Films* **1987**, *148*, 51–65. [CrossRef]
35. Lesage, J.; Chicot, D. A model for hardness determination of thin coatings from standard microindentation test. *Surf. Coat. Technol.* **2005**, *200*, 886–889. [CrossRef]
36. Benarioua, Y.; Mejias, A.; Roudet, F.; Lost, A.; Chicot, D. Hardness-load modeling applied to multilayer galvanized coatings. *Surf. Eng.* **2016**, *32*, 194–200. [CrossRef]
37. Kriger, M.S.; Cook, K.D. Durable gold-coated fused silica capillaries for use in electrospray mass spectrometry. *Anal. Chem.* **1995**, *67*, 385–389. [CrossRef]
38. Popov, K.I.; Živković, P.M.; Jokić, B.; Nikolić, N.D. The shape of the polarization curve and diagnostic criteria for the metal electrodeposition process control. *J. Serb. Chem. Soc.* **2016**, *81*, 291–306. [CrossRef]
39. Berube, L.P.; Esperance, G.L. A Quantitative Method of Determining of the Degree of Texture of Zinc Electrodeposits. *J. Electrochem. Soc.* **1989**, *136*, 2314–2315. [CrossRef]
40. Avramović, L.; Pavlović, M.M.; Maksimović, V.M.; Vuković, M.; Stevanović, J.S.; Bugarin, M.; Nikolić, N.D. Comparative Morphological and Crystallographic Analysis of Electrochemically- and Chemically-Produced Silver Powder Particles. *Metals* **2017**, *7*, 160. [CrossRef]
41. Avramović, L.; Maksimović, V.M.; Baščarević, Z.; Ignjatović, N.; Bugarin, M.; Marković, R.; Nikolić, N.D. Influence of the Shape of Copper Powder Particles on the Crystal Structure and Some Decisive Characteristics of the Metal Powders. *Metals* **2019**, *9*, 56. [CrossRef]

42. Popov, K.I.; Maksimović, M.D. Theory of the Effect of Electrodeposition at a Periodically Changing Rate on the Morphology of Metal Deposits. In *Modern Aspects of Electrochemistry*; Conway, B.E., Bockris, J.O'M., White, R.E., Eds.; Plenum Press: New York, NY, USA, 1989; Volume 19, pp. 193–250. [CrossRef]
43. Popov, K.I.; Djokić, S.S.; Nikolić, N.D.; Jović, V.D. *Morphology of Electrochemically and Chemically Deposited Metals*; Springer International Publishing: New York, UY, USA, 2016.
44. Li, H.; Bradt, R.C. Knoop microhardness anisotropy of single-crystal LaB6. *Mater. Sci. Eng. A* **1991**, *142*, 51–61. [CrossRef]
45. Lamovec, J.; Jović, V.; Mladenović, I.; Stojanović, D.; Kojović, A.; Radojević, V. Indentation behavior of soft film on hard substrate composite system type. *Mater. Prot.* **2015**, *56*, 269–277.
46. Buckle, H. *The Science of Hardness Testing and Its Research Applications*; Westbrook, J.W., Conrad, H., Eds.; American Society for Metals: Metals Park, OH, USA, 1973; p. 453.
47. Nikolić, N.D.; Branković, G.; Maksimović, V.M. Morphology and internal structure of copper deposits electrodeposited by the pulsating current regime in the hydrogen co-deposition range. *J. Solid State Electrochem.* **2012**, *16*, 321–328. [CrossRef]
48. Zhang, J.M.; Ma, F.; Xu, K.W. Calculation of the surface energy of FCC metals with modified embedded-atom method. *Appl. Surf. Sci.* **2004**, *229*, 34–42. [CrossRef]
49. Wang, S.G.; Tian, E.K.; Lung, C.W. Surface energy of arbitrary crystal plane of bcc and fcc metals. *J. Phys. Chem. Solids* **2000**, *61*, 1295–1300. [CrossRef]
50. Reddy, A.K.; Gamboa-Aldeco, M.E. Modern Electrochemistry 2A. In *Fundamentals of Electrodics*; Springer: Boston, MA, USA, 2000; p. 1333. [CrossRef]
51. Nikolić, N.D.; Maksimović, V.M.; Branković, G. Morphological and crystallographic characteristics of electrodeposited lead from the concentrated electrolyte. *RSC Adv.* **2013**, *3*, 7466–7471. [CrossRef]
52. Tao, S.; Li, D.Y. Trbological, mechanical and electrochemical properties of nanocrystalline copper deposits produced by pulse electrodeposition. *Nanotechnology* **2006**, *17*, 65–78. [CrossRef]
53. Ibanez, A.; Fatas, E. Mechanical and structural properties of electrodeposited copper and their relation with the electrodeposition parameters. *Surf. Coat. Technol.* **2005**, *191*, 7–16. [CrossRef]
54. Hall, E.O. The Deformation and Ageing of Mild Steel: III Discussion of Results. *Proc. Phys. Soc. Sec. B* **1951**, *64*, 747–753. [CrossRef]
55. Petch, N.J. The cleavage strength of polycrystals. *J. Iron Steel Inst.* **1953**, *174*, 25–28.
56. Lesage, J.; Pertuz, A.; Puchi-Cabrera, E.S.; Chicot, D. A model to determine the surface hardness of thin films from standard micro-indentation tests. *Thin Solid Films* **2006**, *497*, 232–238. [CrossRef]
57. Lesage, J.; Pertuz, A.; Chicot, D. A New Method to Determine the Hardness of Thin Films. *Matéria* **2004**, *9*, 13–22.
58. Nikolić, N.D.; Rakočević, Z.; Popov, K.I. Structural Characteristics of Bright Copper Surfaces. *J. Electroanal. Chem.* **2001**, *514*, 56–66. [CrossRef]
59. Lamovec, J.; Jović, V.; Ranđelović, D.; Aleksić, R.; Radojević, V. Analysis of the composite and film hardness of electrodeposited nickel coatings on different substrates. *Thin Solid Films* **2008**, *516*, 8646–8654. [CrossRef]
60. Callister, W.D., Jr. *Fundamentals of Materials Science and Engineering*; An Interactive E-text (5th Edition); John Wiley & Sons, Inc.: New York, NY, USA, 2001; p. S-166.
61. Atkinson, M. Calculation of characteristic macro-hardness from low-load indentation test. *Mater. Sci. Eng. A* **1995**, *197*, 165–169. [CrossRef]
62. Popov, K.I.; Pavlović, M.G. Electrodeposition of Metal Powders with Controlled Grain Size and Morphology. In *Modern Aspects of Electrochemistry*; White, R.E., Bockris, J.O'M., Conway, B.E., Eds.; Plenum Press: New York, NY, USA, 1993; Volume 24, pp. 299–391.

© 2020 by the authors. Licensee MDPI, Basel, Switzerland. This article is an open access article distributed under the terms and conditions of the Creative Commons Attribution (CC BY) license (http://creativecommons.org/licenses/by/4.0/).